Hindawi Publishing Corporation
Journal of Nanomaterials
Volume 2011, Article ID 624067, 7 pages
doi:10.1155/2011/624067

Research Article

Characterization and Electrocatalytic Properties of Titanium-Based $Ru_{0.3}Co_{0.7-x}Ce_x$ Mixed Oxide Electrodes for Oxygen Evolution in Alkaline Solution

Hongjun Wu, Qin Ruan, Li Li, and Baohui Wang

Lab of New Energy Chemistry and Environmental Science, College of Chemistry & Chemical Engineering, Northeast Petroleum University, Heilongjiang, Daqing 163318, China

Correspondence should be addressed to Baohui Wang, wangbaohui60@163.com

Received 12 January 2011; Accepted 24 February 2011

Academic Editor: Zhenmeng Peng

Ti-supported RuO_2-Co_3O_4-CeO_2 ($Ru_{0.3}Co_{0.7-x}Ce_x$ oxide, $0 \le x \le 0.7$) electrodes were prepared by sol-gel process. The phase structure, surface morphology, and microstructure of the oxide layer were characterized by X-ray diffraction (XRD) and scanning electron microscopy (SEM). Electrocatalytic activity and oxygen evolution reaction (OER) kinetics on these electrodes in 1.0 mol·dm^{-3} KOH solution were studied by recording open-circuit potential, cyclic voltammetry, and polarisation curves. The results showed that the appropriate content of CeO_2 could reduce the grain size and increase active surface area. The electrocatalytic activity shows a strong dependence on the CeO_2 content in the film. Catalytic performance of mixed oxide electrodes with 40 mol % CeO_2 was the best, with the greatest voltammetric charge, 86.23 mC·cm^{-2}, and the smallest apparent activation energy for OER at 0.60 V was 22.76 kJ·mol^{-1}.

1. Introduction

The oxygen evolution reaction (OER) is one of the most intensively studied electrochemical reactions due to its importance in practical applications such as water electrolysis, chloralkali cells, fuel cells, and secondary metal air batteries. The OER is a very interesting process because of its high activation overpotentials in aqueous solutions. Ruthenium is well known as one of the most active and promising elements, and RuO_2 has been shown to possess interesting electrocatalytic properties for the OER both in acid and alkaline solutions [1–4]. Although RuO_2- and IrO_2-coated Ti electrodes are known to possess high catalytic activity, they lack the stability required for practical applications [5]. The long-term performance of RuO_2 and IrO_2 may be improved by the addition of Co_3O_4 [6, 7]. The interest in these electrode materials is mainly due to low cost, wide disposability, stability in alkaline solution, and good electrocatalytic properties. The performance in alkaline solution of a spinel structure Co_3O_4 electrode can be optimized introducing a small amount of RuO_2, an oxide which itself shows poor stability in alkaline solutions [3, 7]. In many investigations, a third oxide is added to either enhance the selectivity or to optimize the activity, selectivity, and stability. CeO_2 is a promising candidate to modulate the electrocatalytic activity of oxide electrodes due to its high redox potential (Ce^{III}/Ce^{IV}) [4, 8–11]. In this paper, we report the investigation of the influence of nominal cerium dioxide concentration $[CeO_2]_x$, respectively, on surface, kinetics, and electrocatalytic properties of Ti supported $Ru_{0.3}Co_{0.7-x}Ce_x$ oxide electrodes for the OER in alkaline medium.

2. Experimental

2.1. Electrode Preparation. Thin film electrodes of nominal compositions were prepared by the sol-gel process (Calcination: 400°C). The polymeric precursor was prepared by mixing citric acid (CA) (Merck) in ethylene glycol (EG) (Merck) at 60°C. The precursor salt ($RuCl_3 \cdot nH_2O$ (Stream Chemicals), $Co(NO_3)_2 \cdot 6H_2O$ (≥99.0%), and $Ce(NO_3)_3 \cdot 4H_2O$ (≥99.0%)), dissolved in ethanol) was then added slowly, at an M/CA/EG molar ratio of 1 : 3 : 12, where M refers to

ruthenium, cobalt, or cerium ions. After total dissolution of the precursor salt, the temperature was raised to 90°C and kept at this level for 2 hours, under vigorous stirring. The solutions were prepared separately and mixed in the proper nominal ratio of ruthenium, cobalt, and cerium ions. Duplicate samples were prepared for each electrode composition. Sandblasted Ti supports were degreased with alkali solution by ultrasonic and etched for 2 h with boiling 10% (w/w) oxalic acid. The precursor mixtures were applied by brushing on one side of a pretreated Ti support. After application of each coating, the electrode was heated in air to 130°C for 10 minutes, for polymerization to occur, and then fired at 400°C for 10 min. This procedure was repeated until the desired nominal oxide loading (1.5–2.0 mg oxide cm^{-2}) was achieved. The final structure received 1-hour annealing at 400°C. Duplicate samples were prepared for each electrode composition. Details of the electrode preparation and final mounting are described elsewhere [12–14].

2.2. Cell, Equipment, and Solutions. Electrochemical studies were performed using 1.0 mol·dm^{-3} KOH aqueous solution as the supporting electrolyte and prepared volumetrically using Milli-Q plus quality water. Solutions were deaerated before and during each experiment using ultrapurified nitrogen gas. All of the experiments were carried out at room temperature. An experimental setup consisting of a conventional electrolytic cell with a main body (~50 mL), one platinum sheet serving as counterelectrode (2.5 cm × 2.5 cm size), and an Ag/AgCl electrode (CH, 3 mol·dm^{-3} KCl, 0.207 V versus SHE at 25°C) reference electrode was used throughout the experiments.

2.3. Techniques and Instruments. Ti supported $Ru_{0.3}Co_{0.7-x}Ce_x$ oxide layers were characterized through X-ray analysis using a Rigaku D/MAX-2200 Model instrument using Cu (Kα) radiation (λ = 0.15418 nm) from 10 to 70° at a scanning speed of 10°·min^{-1}. Morphological information was attained from scanning electron microscopy (SEM, Shimadzu SSX-550).

The open-circuit potential (E_{oc}) of freshly prepared electrodes was measured during 20 min after electrode immersion in the electrolyte. In all cases, a stationary E_{oc}-value was reached after 15 min. Electrochemical experiments were carried out using a BAS 100 B/W instrumentation. The surface response of the electrodes was examined by cyclic voltammetric curves and potentiodynamic curves. Voltammetric curves were recorded at 50 mV s^{-1} covering the −0.6 and 0.4 V (versus Ag/AgCl in 1.0 mol dm^{-3} KOH) range. The voltammetric charge spent in this potential range was determined by integration of the i/E profiles by Origin (version 8.0) software. When the potential was swept between 0.3 and 0.8 V (versus Ag/AgCl), potentiodynamic curves were recorded in 1.0 mol dm^{-3} KOH at 1 mV s^{-1}.

Reaction-order experiments with respect to OH^- were carried out while keeping the electrode at 0.45 V and 0.75 V for 15 min. These electrode potentials were selected because they fell in the linear current domain of the tafel curves. Experiments were carried out with solutions at several different pOH values obtained by systematic substitution of KOH by $KClO_4$, keeping the total ionic concentration constant at 1.0 mol·dm^{-3}.

3. Results and Discussions

3.1. Morphological Characterization. SEM photomicrographs presented in Figures 1(a), 1(b), 1(d), 1(e), 1(g), and 1(h) show clearly the difference in microporosity among the three samples. It was found that a deposited $Ru_{0.3}Co_{0.7-x}Ce_x$ (x = 0) oxide layer appears to be more or less severely cracked, while $Ru_{0.3}Co_{0.7-x}Ce_x$ (x = 0.4, 0.7) oxide deposits appeared to be more porous.

Figures 1(c), 1(f), and 1(i) show the X-ray diffraction patterns for different compositions of electrodes prepared at 400°C. For all the investigated samples, well-defined Ti peaks can be observed. Because Ti was not previously incorporated into the coating mixture, the presence of these peaks can be attributed to the Ti substrate. As shown in Figure 1(c), the RuO_2 presents a well-defined crystallinity in the rutile form, characterized by the main peaks at the positions 2θ = 28.26° and 35.24°; the Co_3O_4 spinel structures are at 2θ = 18.88°, 30.98°, 36.98°, 54.94°, and 58.94°. On the other hand, the different values of the crystallographic parameters between the RuO_2 rutile and the Co_3O_4 spinel structures lead low probability to forming a solid solution.

Compared with the non-CeO_2 electrodes, diffractograms of mixed oxide films exhibit somewhat broader peaks suggesting a lower crystallinity of active component as shown in Figures 1(f) and 1(i). The results show that CeO_2 does not form solid solutions with the rutile phase (e.g., RuO_2 and TiO_2), acting solely as a dispersant matrix for this phase, which is expected to lead to a strong increase of the electrochemically active surface area [10].

3.2. Open-Circuit Potential. Figure 2 shows the dependence of the open potential, E_{oc}, on the film composition for freshly prepared electrodes, measured in 1.0 mol·dm^{-3} KOH. RuO_2 and Co_3O_4 are both active materials for oxygen evolution reaction. As shown in Figure 2, introduction of CeO_2 into the binary RuO_2 and Co_3O_4 mixture causes a slight increase in E_{oc}.

3.3. Voltammetric Curves. Figure 3 shows representative voltammetric curves of the electrodes at different CeO_2 content. A substitute of 40 mol% Co_3O_4 by CeO_2 leads to a significant increase in the voltammetric current density; as the concentration of CeO_2 increases, the symmetry of redox peaks increases. The band located at ~0.27 V is attributed to the Ru^{III}/Ru^{IV} redox couple. As discussed by Fernandes [15], the nonsymmetric profile of the broadbands located in the −0.6 to −0.3 V interval, which are also present in alkaline solution, can be correlated with a slow irreversible Faradaic reduction occurring on the oxide surface. The apparent irreversibility of the surface solid-state redox transitions can be associated with the instability of a small electrode. But it is denounced by the nonsymmetric profile of the broadbands located in the more cathodic region [15, 16].

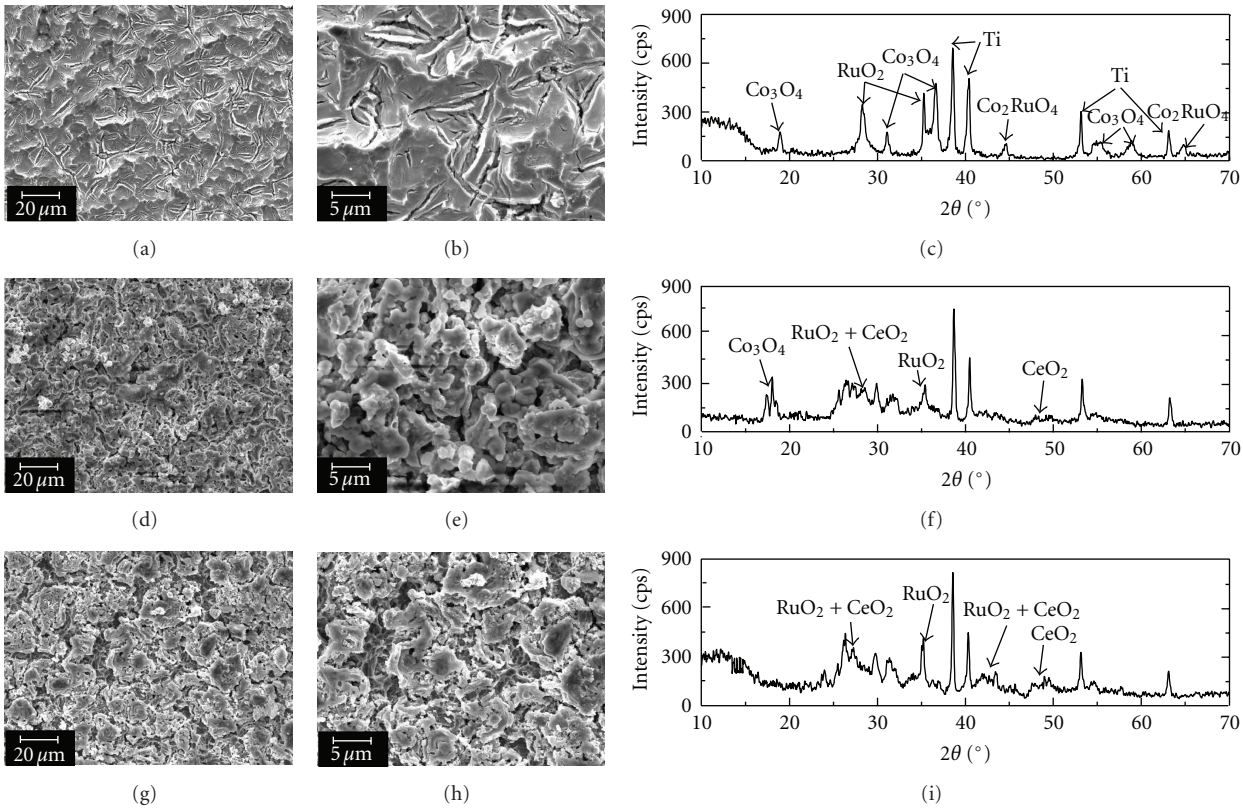

FIGURE 1: XRD patterns and SEM images of the surface of $Ru_{0.3}Co_{0.7-x}Ce_x$ oxide electrodes (a, b, c) $x = 0.0$; (d, e, f) $x = 0.4$; (g, h, i) $x = 0.7$.

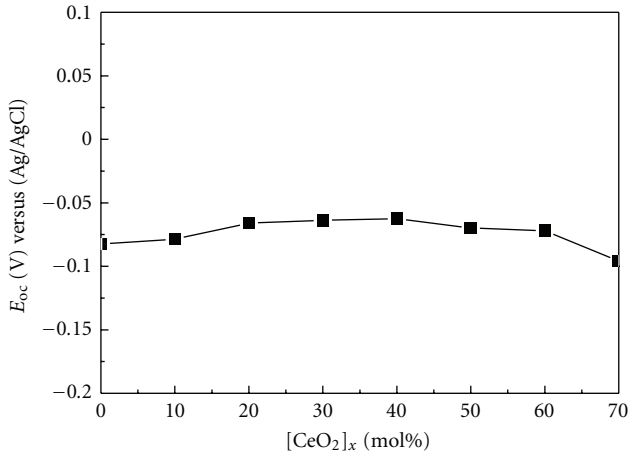

FIGURE 2: Open-circuit potential on the nominal CeO_2 content in 1.0 mol·dm^{-3} KOH.

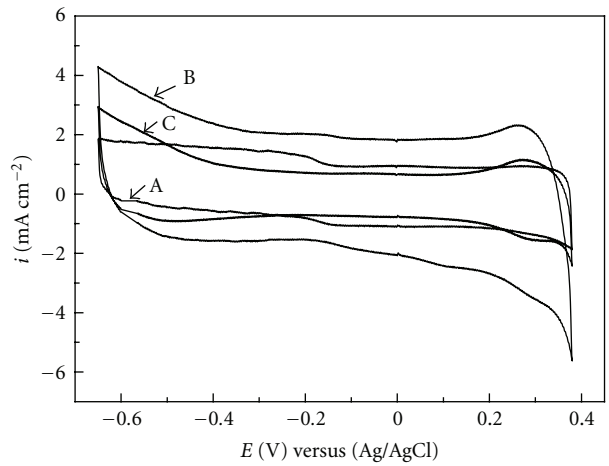

FIGURE 3: Voltammetric curves of Ti/ $Ru_{0.3}Co_{0.7-x}Ce_x$ oxide electrodes with different molar content of CeO_2 in 1.0 mol/L KOH at 50 mv s^{-1}. (a) $x = 0.0$; (b) $x = 0.4$; (c) $x = 0.7$.

When the integration of anodic and cathodic currents of the voltammetric profile is limited to more anodic regions, the ratios of q_a/q_c-ratios ≥ 0.956, for all the oxide compositions. This high ratio close to unity indicates that the oxide surface is stable under the conditions applied during this work. Therefore, the addition of the CeO_2 could be related to an increase in the surface area possibly by the mechanisms of the inhibition of the grain growth process or a decrease in the sintering process rate.

The voltammetric charge was obtained by integration of voltammetric cures and is plotted as a function of CeO_2 content in Figure 4. The only processes occurring in the

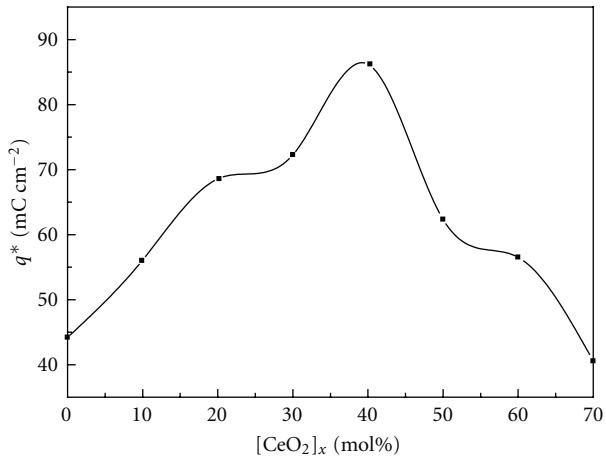

Figure 4: Voltammetric charge (q^*) on the nominal CeO_2 content.

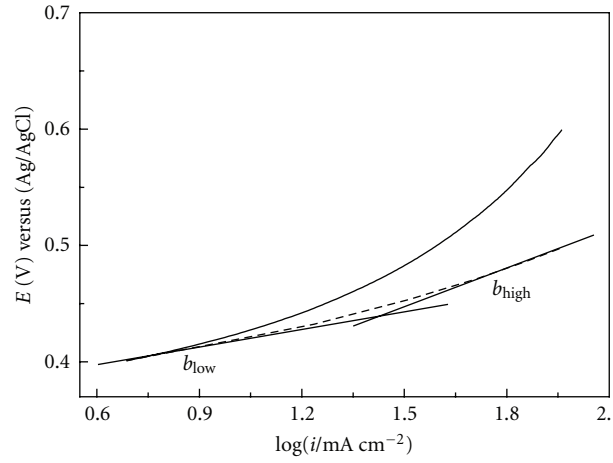

(a)

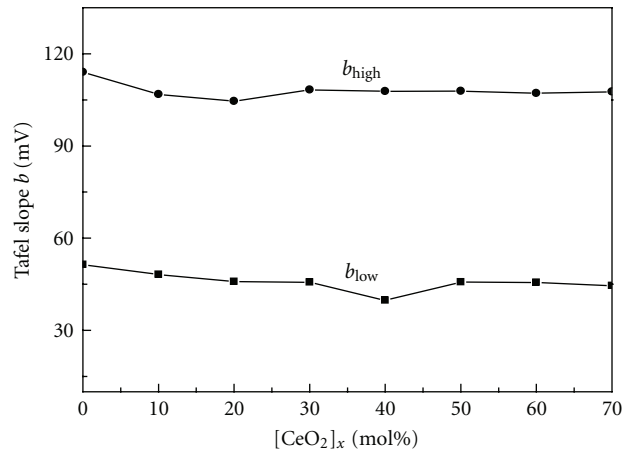

(b)

Figure 5: (a) Representative tafel plot of the OER; (b) dependence of tafel slope on $[CeO_2]_x$ in the low overpotential region, b_{low}, and high overpotential region, b_{high}.

$-0.6\sim0.4$ V potential range are the surface redox transitions of Ru species and double-layer charging at the oxide-solution interface. Since the latter is as a rule small compared to the former, it measures the number of surface area active sites. This is different from the concept of surface area that also includes Ti-containing sites, but it can be defined as proportional to the electrochemically active surface area [17].

Figure 4 shows that for fresh electrodes q^* goes through a maximum at about 40 mol% CeO_2. This can be related with morphological and microstructural changes due to the oxide mixture. As the anodic charge is proportional to the number of electrochemically active sites in the electrode surface, and CeO_2 presents no electrochemical activity in this potential range, it is proposed that the voltammetric charge is a function of RuO_2 active sites density in the electrode surface, related to an increase in the surface area possibly by the mechanisms of the inhibition of the grain growth process and/or a decrease in the sintering process rate. But the excess content of CeO_2 destructs the integrity of the lattice and impacts the surface active areas.

3.4. Oxygen Evolution Reaction

3.4.1. Tafel Lines. The obtained tafel plots showed a deviation from the linearity at high overpotentials. A linear tafel plot should be expected in the studied potential range, in the absence of an ohmic drop expressed as IR_Ω. This IR_Ω value was used to fit the corrected ohmic drop polarization curve at high overpotential [18]. The influence of ohmic drop, IR_Ω, on the polarization curve can be written as

$$E - IR_\Omega = a + b \log i, \tag{1}$$

where R_Ω is the total ohmic resistance, E is the electrode potential, a is the constant, and b is the tafel slope.

Figure 5(a) shows a typical quasistationary potential sweep curve before and after IR_Ω correction. The optimum R_Ω values randomly distributed in the 0.2–1.8 Ω interval were obtained. The R_Ω values found are in excellent agreement with other RuO_2-based oxide electrodes submerged in similar supporting electrolyte [15]. As the resistance of the film is negligible due to the metallic conductor nature of RuO_2, the R_Ω values can be attributed only to the solution resistance.

After the ohmic drop correction, all curves show two linear regions for all the investigated electrodes. Figure 5(b) gathers tafel slope data, b, determined in the low and high overpotential domains as a function of $[CeO_2]_x$. Tafel data reveal that the influence of $[CeO_2]_x$ on OER kinetics strongly depends on the overpotential domain. This behaviour is in agreement with literature reports [19] on oxide electrodes containing noble metals (e.g., Ru and Ir) as the active component. Figure 6 clearly shows that tafel slopes in the low and high overpotential domains, b_{low} and b_{high}, are little affected by the $[CeO_2]_x$. At low overpotentials, tafel slopes close to 50 mV were observed. At high overpotentials, after IR_Ω correction, a second tafel slope is observed randomly distributed around 120 mV for all compositions. The change of the tafel slope indicates that deviation of the experimental

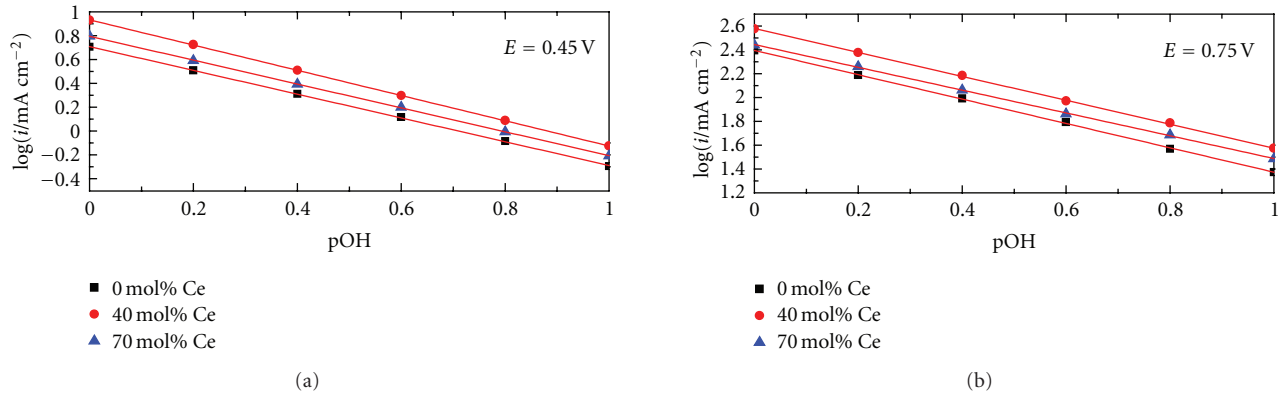

Figure 6: Dependence of current density, i, on pOH. (a) $E = 0.45$ V; (b) $E = 0.75$ V.

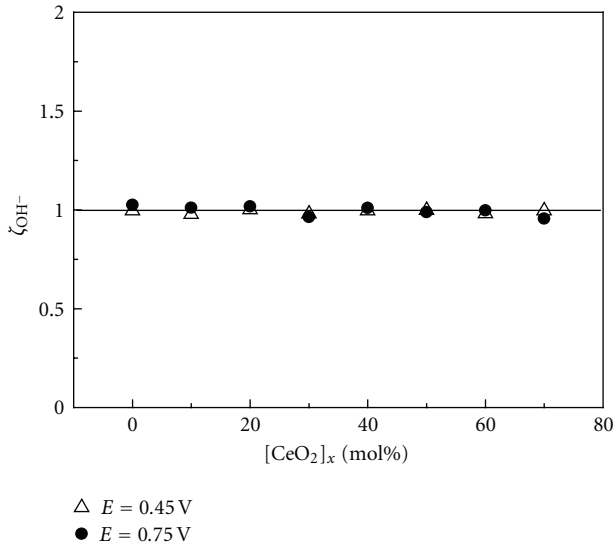

Figure 7: Influence of $[CeO_2]_x$ on reaction order with respect to OH^-, ζ_{OH^-}. Electrolyte: $[KClO_4] + [KOH] = 1.0$ mol/L.

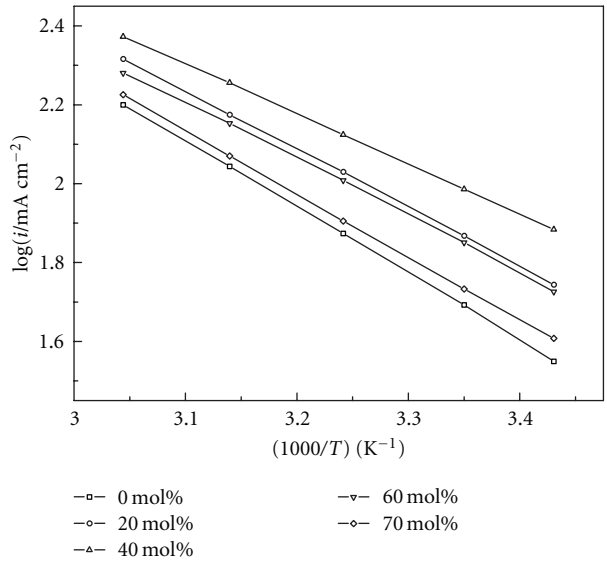

Figure 8: OER Arrhenius plots on different content of CeO_2 electrodes at 0.6 V versus Ag/AgCl.

data from linearity is due to ohmic drop resistance combined with a change in the electrode mechanism (or its rate-determining step, rds).

3.4.2. Reaction Order with Respect to OH^-, ζ_{OH^-}. Reaction order determination provides useful information to elucidate the electrode mechanism. The reaction order with respect to OH^-, ζ_{OH^-}, was determined in both the low and high overpotential domains as a function of nominal oxide composition. To be significant, reaction orders must be determined at constant ionic strength to avoid diffuse double-layer effects [19]. To accomplish this, KOH concentration was varied between 0.1 and 1.0 mol·dm^{-3} keeping the ionic strength constant at 1.0 mol·dm^{-3} by systematic substitution of OH^- by ClO_4^- ions.

Keeping constant the electrode potential and considering negligible changes in water activity, the reaction order with respect to OH^-, ζ_{OH^-}, for conditions of the high-field approximation, $\eta \geq 0.1$ V, was determined using next equation:

$$\zeta_{OH^-} = -\left[\frac{\partial \log i}{\partial \mathrm{pOH}}\right]_{E,T}, \quad (2)$$

where $\mathrm{pOH} = -\log[OH^-]$.

Representative plots of current density as a function of OH^- concentration at constant ionic strength are reported in Figure 6 for both low (0.45 V) and high (0.75 V) overpotentials.

Figure 6 clearly shows that the linear segments in the log i versus pOH plots are parallel, revealing that ζ_{OH^-} values are independent of $[CeO_2]_x$. Figure 7 presents the ζ_{OH^-} data as function of $[CeO_2]_x$ showing the data are randomly scattered around unity on changing $[CeO_2]_x$ ($\zeta_{OH^-} \approx 1$ in all cases), which show that the reaction order with respect to OH^- does

Table 1: OER apparent activation energy of electrodes with different content of CeO_2 at 0.6 V versus Ag/AgCl.

$[CeO_2]_x$/mol%	0	10	20	30	40	50	60	70
ΔE_a/(kJ/mol)	32.16	31.54	28.26	31.09	22.76	26.17	27.47	30.62

not vary with the concentration of OH^- and the content of CeO_2.

3.5. Apparent Activation Energy. The effect of temperature on the kinetic parameters of the electrocatalyst is of paramount importance for the oxygen evolution reaction of anode. The influence of temperature on the kinetics of oxygen reduction was examined by linear sweep voltammetry (LSV) measurements at different temperature ranging from 18°C to 55°C. The apparent activation energy, ΔE_a, for the oxygen reduction reaction on Ti/Ru-Co-Ce cluster catalyst was calculated from a linear regression analysis of the slope of the Arrhenius equation represented by the following relationship:

$$i = k\exp\left[\frac{(-\Delta E_a)_\eta}{RT}\right] \longrightarrow (\Delta E_a)_\eta = -2.303R\left[\frac{\partial(\log i)}{\partial(1/T)}\right]. \quad (3)$$

Representative plots of current density as a function of T at constant overpotential (0.6 V) are reported in Figure 8. Figure 8 clearly shows that the linear correlation coefficient could be very close to one ($r > 0.999$). Also, for all catalysts, the current densities increase rapidly with the increase of temperature. The enhanced reaction rate is reasonably understood in that elevated temperature. According to slope from Figure 8, we can calculate ΔE_a for each electrode (see Table 1). The doping of CeO_2 can decrease the apparent activation energy of OER; the electrode with 40 mol% CeO_2 has the smallest ΔE_a which is 22.76 kJ/mol.

4. Conclusions

XRD study shows that CeO_2 does not form solid solutions with the rutile phase (e.g., RuO_2 and TiO_2), only acts as a dispersant, and causes diffractograms with somewhat broader peaks and a strong increase in the oxide surface roughness, suggesting a lower crystallinity and higher surface area of active component.

"In situ" studies of the conductive metallic oxide electrodes reveal that an introduction of CeO_2 into the binary RuO_2 and Co_3O_4 mixture changes the electrode morphology and surface properties, increasing the electrode surface area and slightly increasing E_{oc}. Electrocatalytic activity of electrodes with 40 mol% CeO_2 nominal composition is the best, with the greatest voltammetric charge, 86.23 $mC\cdot cm^{-2}$, and the smallest apparent activation energy for OER at 0.60 V was 22.76 kJ/mol.

The kinetic study of the OER revealed that while overpotential domain affects the electrode process, it is unrelated to CeO_2. Experimental tafel slope and reaction order data with respect to $[OH^-]$, combined with the theoretical analysis based on the concept of the apparent electronic transfer coefficient, support the electrode mechanism proposed by Yeager adequately describes the OER in alkaline medium. Experimental tafel slopes at low and high overpotentials were 40 mV and 120 mV, respectively. The reaction orders with respect to $[OH^-]$ are both 1.0.

Acknowledgments

This work was supported by the National Natural Science Foundation of China (no. 50476091) and Natural Science Foundation of Heilongjiang Province (no. B200401).

References

[1] S. Licht, B. Wang, S. Mukerji, T. Soga, M. Umeno, and H. Tributsch, "Efficient solar water splitting, exemplified by RuO_2-catalyzed AlGaAs/Si photoelectrolysis," *Journal of Physical Chemistry B*, vol. 104, no. 38, pp. 8920–8924, 2000.

[2] S. Licht, B. Wang, S. Mukerji, T. Soga, M. Umeno, and H. Tributsch, "Over 18% solar energy conversion to generation of hydrogen fuel; theory and experiment for efficient solar water splitting," *International Journal of Hydrogen Energy*, vol. 26, no. 7, pp. 653–659, 2001.

[3] N. Krstajic and S. Trasatti, "Cathodic behaviour of RuO_2-doped Ni/Co_3O_4 electrodes in alkaline solutions: hydrogen evolution," *Journal of Applied Electrochemistry*, vol. 28, no. 12, pp. 1291–1297, 1998.

[4] L. A. De Faria, J. F. C. Boodts, and S. Trasatti, "Electrocatalytic properties of ternary oxide mixtures of composition $Ru_{0.3}Ti_{(0.7-x)}Ce_xO_2$: oxygen evolution from acidic solution," *Journal of Applied Electrochemistry*, vol. 26, no. 11, pp. 1195–1199, 1996.

[5] C. Iwakura and K. Sakamoto, "Effect of active layer composition on the service life of (SnO_2 and RuO_2)-coated Ti electrodes in sulfuric acid solution," *Journal of the Electrochemical Society*, vol. 132, no. 10, pp. 2420–2423, 1985.

[6] L. A. De Faria, M. Prestat, J. F. Koenig, P. Chartier, and S. Trasatti, "Surface properties of Ni-Co mixed oxides: a study by X-rays, XPS, BET and PZC," *Electrochimica Acta*, vol. 44, no. 8-9, pp. 1481–1489, 1998.

[7] R. N. Singh, J. P. Pandey, N. K. Singh, B. Lal, P. Chartier, and J. F. Koenig, "Sol-gel derived spinel $M_xCo_{3-x}O_4$ (M = Ni, Cu; $0 \le x \le 1$) films and oxygen evolution," *Electrochimica Acta*, vol. 45, no. 12, pp. 1911–1919, 2000.

[8] L. A. De Faria, J. F. C. Boodts, and S. Trasatti, "Electrocatalytic properties of Ru + Ti + Ce mixed oxide electrodes for the Cl_2 evolution reaction," *Electrochimica Acta*, vol. 42, no. 23-24, pp. 3525–3530, 1997.

[9] V. A. Alves, L. A. Da Silva, and J. F. C. Boodts, "Surface characterisation of $IrO_2/TiO_2/CeO_2$ oxide electrodes and Faradaic impedance investigation of the oxygen evolution reaction from alkaline solution," *Electrochimica Acta*, vol. 44, no. 8-9, pp. 1525–1534, 1998.

[10] L. M. Da Silva, K. C. Fernandes, L. A. De Faria, and J. F. C. Boodts, "Electrochemical impedance spectroscopy study during accelerated life test of conductive oxides: Ti/(Ru + Ti + Ce)O_2-system," *Electrochimica Acta*, vol. 49, no. 27, pp. 4893–4906, 2004.

[11] L. A. De Faría, J. F. C. Boodts, and S. Trasatti, "Physicochemical and electrochemical characterization of Ru-based ternary oxides containing Ti and Ce," *Electrochimica Acta*, vol. 37, no. 13, pp. 2511–2518, 1992.

[12] J. Ribeiro and A. R. De Andrade, "Characterization of RuO_2 – Ta_2O_5 coated titanium electrode microstructure, morphology, and electrochemical investigation," *Journal of the Electrochemical Society*, vol. 151, no. 10, pp. D106–D112, 2004.

[13] J. Ribeiro and A. R. de Andrade, "Investigation of the electrical properties, charging process, and passivation of RuO_2 – Ta_2O_5 oxide films," *Journal of Electroanalytical Chemistry*, vol. 592, no. 2, pp. 153–162, 2006.

[14] J. Ribeiro, M. S. Moats, and A. R. De Andrade, "Morphological and electrochemical investigation of RuO_2 – Ta_2O_5 oxide films prepared by the Pechini-Adams method," *Journal of Applied Electrochemistry*, vol. 38, no. 6, pp. 767–775, 2008.

[15] K. C. Fernandes, L. M. D. Silva, J. F. C. Boodts, and L. A. De Faria, "Surface, kinetics and electrocatalytic properties of the Ti/(Ti + Ru + Ce)O_2-system for the oxygen evolution reaction in alkaline medium," *Electrochimica Acta*, vol. 51, no. 14, pp. 2809–2818, 2006.

[16] L. A. De Faría, J. F. C. Boodts, and S. Trasatti, "Physicochemical and electrochemical characterization of Ru-based ternary oxides containing Ti and Ce," *Electrochimica Acta*, vol. 37, no. 13, pp. 2511–2518, 1992.

[17] S. Trasatti, "Physical electrochemistry of ceramic oxides," *Electrochimica Acta*, vol. 36, no. 2, pp. 225–241, 1991.

[18] L. M. Da Silva, J. F. C. Boodts, and L. A. De Faria, "Oxygen evolution at $RuO_2(x)$ + $Co_3O_4(1 - x)$ electrodes from acid solution," *Electrochimica Acta*, vol. 46, no. 9, pp. 1369–1375, 2001.

[19] V. Consonni, S. Trasatti, F. Pollak, and W. E. O'Grady, "Mechanism of chlorine evolution on oxide anodes study of pH effects," *Journal of Electroanalytical Chemistry*, vol. 228, no. 1-2, pp. 393–406, 1987.